Available online at www.sciencedirect.com

ScienceDirect

journal homepage: www.elsevier.com/locate/he

# Steam reforming of $CH_4$ at low temperature on Ni/$ZrO_2$ catalyst: Effect of $H_2O/CH_4$ ratio on carbon deposition

Qing Zhao [a], Ye Wang [b], Yannan Wang [a], Li Li [a], Wenqing Zeng [b], Guiying Li [a,**], Changwei Hu [a,b,*]

[a] Key Laboratory of Green Chemistry and Technology, Ministry of Education, College of Chemistry, Sichuan University, Chengdu, Sichuan, 610065, PR China

[b] College of Chemical Engineering, Sichuan University, Chengdu, Sichuan 610065, PR China

## HIGHLIGHTS

- When $H_2O/CH_4$ = 2, Ni/$ZrO_2$ exhibited the highest $CH_4$ conversion (46.8%) at 550 °C.
- Polymer carbon and fiber carbon both formed at low $H_2O/CH_4$ ratio(1, 2, 3).
- Only polymer carbon formed at high $H_2O/CH_4$ ratio(5, 10).
- Easy to removal polymer carbon($C_1$) covered the active site at low $H_2O/CH_4$ ratio.
- The excess water would lead to the conversion of $Ni^0$ to $Ni(OH)_2$.

## GRAPHICAL ABSTRACT

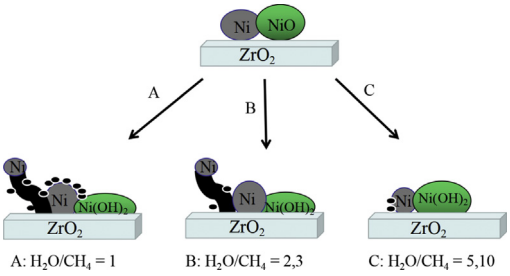


## ARTICLE INFO

*Article history:*
Received 22 January 2020
Received in revised form
10 March 2020
Accepted 16 March 2020
Available online 11 April 2020

*Keywords:*
Methane steam reforming

## ABSTRACT

In present work, the $H_2O/CH_4$ on carbon deposition in SRM reaction over Ni/$ZrO_2$ was studied. Prepared by impregnation, the catalysts were characterized by TEM, XPS, $H_2$-TPR, TG-DSC-MS, Raman, and XRD. The results showed that when $H_2O/CH_4$ = 2 with GHSV of 14460 $h^{-1}$, the highest $CH_4$ conversion (46.8%) was achieved on the Ni/$ZrO_2$ catalyst at 550 °C. This was due to the relatively high surface content of $Ni^0$ (27%) species and the formation of easy removal polymer carbon ($C_1$). When the $H_2O/CH_4$ was 1, a large amount of difficult to remove fiber carbon ($C_2$) formed and polymer carbon would wrap around the catalyst to reduce its activity. However, excess water might promote surface reconstruction by converting $Ni^0$ to

* *Corresponding author*. Key Laboratory of Green Chemistry and Technology, Ministry of Education, College of Chemistry, Sichuan University, Chengdu, Sichuan, 610065, PR China.
** *Corresponding author*.
E-mail addresses: liguiying@scu.edu.cn (G. Li), changweihu@scu.edu.cn (C. Hu).
https://doi.org/10.1016/j.ijhydene.2020.03.112

Carbon deposition
Nickel
Zirconia
Low temperature

$Ni(OH)_2$, which reduced the surface $Ni^0$ content and then inhibited the catalytic activity, while the amount of carbon deposited, especially $C_2$, reduced significantly.



## Introduction

Energy shortages and environmental pollution have become bottlenecks restricting the development of world economy. In order to reduce energy consumption and alleviate urban pollution, fuel cells are developing rapidly in recent years. As an alternative to fossil fuels, hydrogen is becoming more and more important in the 21st century [1–5]. Especially in the field of electric vehicles, hydrogen fuel cells play an important role [6–8], because the chemical reaction of hydrogen in fuel cells only produce water vapor. In literature, there are four main ways to produce hydrogen: electrolysis, photolysis, biological solution and pyrolysis [9–13]. Although methane partial oxidation, catalytic combustion, and electrolysis technologies are developing rapidly, steam reforming of natural gas is still the primary technology for large scale hydrogen production [14,15]. Methane has the highest hydrogen to carbon ratio, and is the most suitable hydrogen production material. To date, there are many methods to produce $H_2$ from $CH_4$ including steam reforming [2,16–18], $CO_2$ reforming [19], autothermal reforming [20], and triple reforming [21]. Compared with other reactions, methane steam reforming is more widely used in industrial applications, because it does not require oxygen and the raw materials are readily available [22]. Because CO water shift reaction usually occurs simultaneously, a higher hydrogen yield is obtained [23,24]. One of the limitations of SMR reaction is that the endothermic reaction needs high temperature, generally higher than 800 °C [25], which increases the cost of operation. High reaction temperature will also lead to lower thermal efficiency of the process. Milder reaction condition could contribute to low energy cost. M.H. Halabi et al. [26] found that the main gas products were $CO_2$ and $H_2$ instead of CO at low temperature (475°C–725 °C), which was due to the fact that water gas shift reaction was benefited at low temperature, implying that higher yield of hydrogen could be achieved. Therefore, low temperature methane steam reforming is still of great research significance [27,28].

Another limitation in the pragmatic production was carbon deposition. Especially, using Ni based catalysts, serious carbon deposition was often caused by the decomposition of methane for SRM reaction at low temperature [29–31]. Several researches on carbon deposition to improve the catalytic activity were reported [32–36]. It has been reported that improving the interaction between metal Ni and the support could reduce the formation of carbon [37]. Low temperature SMR reaction over Ni-$Ce_{(1-x)}Zr_xO_2$ catalyst could be carried out under severe conditions ($H_2O/CH_4$ = 1) [38]. The mixed $Ce_{0.8}Zr_{0.2}O_2$ solid had the synergy effect, resulted from high Ni dispersion, strong thermal resistance, and enhanced reducibility. 15 wt% Ni-$Ce_{0.8}Zr_{0.2}O_2$ showed the best activity and stability at 600 °C. Hak-Min Kim et al. [28] investigated the performance of Ni-$Ce_{0.8}Zr_{0.2}O_2$ catalysts promoted by basic metal oxide(MgO, CaO, and $La_2O_3$) prepared by co-precipitation method for SMR reaction at low temperature (600 °C). It was found that the basicity and the interaction degree of metal with support influence the carbon deposition [28,39]. Due to its high Ni dispersion, strong basicity, and metal-support interaction, La-Ni-$Ce_{0.8}Zr_{0.2}O_2$ showed the best catalytic activity.

Moreover increasing water to methane ratio can effectively eliminate some carbon deposition, and the low steam conditions resulted in ineffective carbon gasification [40]. However, excessive water will lead to the reduction of process thermal efficiency and the change of product composition. Therefore, optimization of water to methane ratio can not only obtain better conversion rate, selectivity and yield, but also effectively inhibit the carbon deposition to a certain extent. At present, many studies have reported the effects of different water-methane ratio on catalytic activity [41–43]. Ee Teng Kho [23] et al. assessed the stability of Ni/$TiO_2$ in SMR at $H_2O/CH_4$ ratios of 1–3 and found that the presence of carbon whiskers at $H_2O/CH_4$ ratios of 2 would deactivate the catalyst. María A [44] proved that the strong interaction between active species and spinel-like matrix could reduce carbon deposition. Kowit Lertwittayanon et al. [45] found that encapsulating carbon or carbon nanotube would form on $CaZrO_3$-modified Ni/α-$Al_2O_3$ catalysts. However, there are few studies on the forms of carbon deposited under different water-methane ratios and the effect on catalytic activity, which needs more comprehensive study.

$ZrO_2$ is a mainly acidic, certain amphoteric character and reducing metal oxide. Zirconium oxide is widely used in heterogeneous catalysis because of its unique properties. Gonzalez et al. [46] discussed the variation of nickel metal particle size under the treatment of $H_2$ or CO with modified nickel/$ZrO_2$ catalyst. Dominik Eder et al.[47] found that $ZrO_2$ can be reduced by hydrogen forming oxygen vacancies in the structure and the presence of water can modify this production. Furthermore, the catalytic activity of surface oxygen vacancy of reduced zirconia for the hydrodeoxygenation reaction of propan-2-ol was also confirmed. Furthermore, it was found that $ZrO_2$ could change the nature of dry reforming of methane reactive sites and promote the formation of active sites for low temperature DRM reaction [48,49]. Because Ni-Si/$ZrO_2$ catalyst showed good activity in methane low temperature reforming reaction [48], we applied this catalytic system to methane steam reforming at low temperature in an attempt to achieve good catalytic activity. In this context, the present work was conducted to look into the influence of the water-methane ratio to carbon deposition on steam methane

reforming over Ni/$ZrO_2$ catalyst. Furthermore, the relationship between catalyst structure and catalytic activity caused by different water-to-methane ratio was further studied. The states of nickel and deposited carbon over the surface of Ni/$ZrO_2$ catalyst were studied in detail.

## Experimental

### *Preparation of catalyst*

Precipitation method was applied to prepare the $ZrO_2$ support. Desired amount of $Zr(NO_3)_4$▪$5H_2O$ (ChengduKelong, China) was dissolved in deionized water with constant stirring. Then, $NH_3 \cdot H_2O$ was added to the above solution to achieve a pH of 9. After stirring for 2 h, the resultant system was aged for 24 h. Then, the mixture was filtered and washed three times with deionized water at room temperature. The obtained sample was dried at 110 °C for 4 h and then calcined at 600 °C for 5 h to obtain the $ZrO_2$ support [48].

The Ni/$ZrO_2$ catalyst (5 wt%) was prepared by impregnation. $Ni(NO_3)_2$▪$6H_2O$ (ChengduKelong, China, 0.9864 g) is added to deionized water (20 mL). The $ZrO_2$ support (4 g) was impregnated with the aforesaid aqueous solution for 24 h at room temperature, then dried at 80 °C for 2h and 110 °C for 4h. After calcination in flowing air at 600 °C for 5 h (with the heating rate of 2 °C/min), the Ni/$ZrO_2$ catalyst precursor was obtained.

### *Catalytic performance test*

The low temperature SRM reaction was performed in a stainless steel fixed bed reactor with 14 mm inner diameter at atmospheric pressure. Firstly, the inert silica filler was added (44 g, 20–40 mesh), then the mixture of the filler and catalyst ($m_{cat.}$ = 0.5 g, 20–40 mesh, 0.25 mL; $m_{silica}$ = 20 g, 20–40 mesh, 7.6 mL) were added, and finally silica filler was added to cover the catalyst bed. The reaction system was heated up to 600 °C (10 °C/min) in argon atmosphere, and then reduced for 1 h in $H_2$/Ar = 1 mixture. After cooling to 550 °C in argon atmosphere, the reaction gases methane (F = 30 mL/min) and $H_2O$ were vented for SMR reaction. While the $H_2O/CH_4$ molar ratio was varied, both methane and argon flow remained at 30 mL/min. Water was injected through a micro pump and then through a preheater at 135 °C after gasification of the carburetor at 135 °C before entering the reactor. The effluent from reactor passes through a condensing device, and a gas chromatography is used for on-line analysis (TDX - 01 packed column) of the gas products. The total flow of effluent was measured by one mass flowmeter. The catalyst and inert filler after reaction are completely in different form and color, and they can be clearly distinguished. The inert filler was a gray, clean ball, and the catalyst was a small particle (black after the reaction). After the reaction, the catalyst can be picked out one by one.

The conversion of methane ($X_{CH4}$), the yield of $H_2$ ($Y_{H2}$) and the content of $H_2$, CO and $CO_2$ ($C_{i(i=H2,CO,CO2)}$)were calculated by the following:

$$XCH4 = \frac{FCH4,\text{in} - FCH4,out}{FCH4,\text{in}}$$

$$YH2 = \frac{2FH2,out}{3(FCH4,in + FH2O,in)} \times 100$$

$$Ci = \frac{Fi,out}{\sum_{i=H2,CO,CO2} Fi,out} \times 100\%$$

where F represents molar flow rate (mol▪$s^{-1}$).

### *Catalyst characterization*

The actual Ni loading of the fresh catalyst was determined by ICP-OES (Agilent, 5100 SVDV). Before the test, the solid catalyst was dissolved in aqueous sulfuric acid with a volume ratio of 1:2 (water/sulfuric acid concentrated) at 240 °C, and a small amount of hydrofluoric acid was added until complete dissolution.

The temperature programmed $NH_3$ adsorption-desorption experiment was carried out to study acid site distribution and strength for the catalysts. The samples were first purged with a flow rate of 25 mL/min He gas, and then heated to 500 °C at a rate of 10 °C/min, and a constant temperature at 500°Cwas kept for 30 min, then cooled down to 50 °C. After switching He to $NH_3$, the adsorption of $NH_3$ (25 mL/min) was endured for 240min. And then switching $NH_3$ to He (25 mL/min) for purging, the temperature was raised to 600 °C at a rate of 10 °C/min, and the $NH_3$ desorption temperature curve was obtained.

The reducibility of calcined samples was obtained by $H_2$ temperature programmed reduction (TPR) method. 0.10g catalyst was pretreated with Ar flow at 150 °C for 30min. The TPR experiment was conducted from 50 °C to 950 °C in $H_2$/Ar (10/90 vol%) flow. TCD detector was used to monitor $H_2$ consumption.

X-ray powder diffraction (XRD) characterization of the catalysts were performed by an XRD-6100 (SHIMADZU) instrument which used Cu K$\alpha$ radiation under the condition of 40 kV and 25 mA. The test range of diffraction angle (2$\theta$) is from 20° to 80°, the scan speed was 0.3s $step^{-1}$, and the step size was 0.03°. Because of the overlap of the XRD profiles of $ZrO_2$ and Ni, the crystal size of them were obtained by Scherrer's equation via splitting of the peaks.

Thermogravimetric and mass spectrometry were used to detect deposited carbon, using NETZSCH TG209F1 instrument. The test temperature range was from 30 °C to 800 °C (10 °C/$min^{-1}$) in air/Ar flow (20/60 mL/$min^{-1}$).

Raman spectra characterization of the used catalysts were carried out by a LabRAM HR Raman Spectrometer (HORIBA Jobin Yvon), which used a He-Ne laser source (532 nm). The Grating was 600 and the filter was D1 with the hole of 200 mm.

An Tecnai G2 F20 machine Twin instrument Transmission (0.2 nm resolution) was used to characterize the used catalysts. In the operation, the acceleration voltage was 200Kv.

X-ray photoelectron spectroscopy (XPS) characterization was performed on AXIS Ultra DLD (KRATOS) spectrometer. All the results were obtained using monochromated Al K$\alpha$ radiation with the accelerating power of 25 W. C 1s 284.6eV was used for calibration, and Lorentz-Gauss ratio (L/G) for peak splitting was 20%.

## Results and discussion

### Ni species reduction

Hydrogen temperature programmed reduction was used to characterize the reduction performance of $Ni/ZrO_2$ precursor and $ZrO_2$(Fig. 1). There was one main peak on the precursor oxide reduction curve. It had been reported that the reduction peak around 400 °C was regarded as bulk NiO species [28]. Therefore, the reduction peak at 420 °C was assigned to bulk NiO. Since there was only a small amount of zirconia carrier surface reduction, the other two shoulder peaks at 308 °C and 342 °C were attributed to the reduction of the surface NiO [50,51]. R. Pérez-Hernández [52] et al. found that the TPR profile of the fresh $NiO/ZrO_2$ sample showed a peak at 320 °C. Hyun-Seog Roh et al. [53] found that the broad reduction peak at about 400 °C was attributed to relatively free NiO weakly interacting with support and the other peak at 510 °C was attributed to complex NiO strongly interacting with support. Evidently, compared with others, the interaction of NiO with the support over the $Ni/ZrO_2$ catalyst was weak.

Dominik Eder et al. [47] found that oxygen vacancies formed when zirconia was reduced with hydrogen. At reduction below 800 K, the oxygen vacancies were most likely located on the zirconia surface while above 800 K, the formation of bulk vacancies started. There were two peaks on the zirconia reduction curve. Therefore, it could be inferred that low temperature reduction peak (389 °C) corresponded to surface oxygen defect ($2.37 \times 10^{-2}$mmol/g) and high temperature reduction peak (627 °C) corresponded to bulk oxygen defect ($3.8 \times 10^{-2}$mmol/g). Therefore, it will form surface oxygen vacancy and part of bulk oxygen vacancy on zirconia under hydrogen reduction at 600 °C.

### The acidity of support and catalyst

The $NH_3$-TPD results showed that there are two type of acidic sites with different strengths of acidity (Fig. 2). The low temperature desorption peak (Tm = 50–200 °C) corresponded to the weak acid sites, and the medium temperature peak (Tm = 200–400 °C) corresponded to the medium acid sites [54,55]. The strength of acid in both $ZrO_2$ and $Ni/ZrO_2$ samples were the same, since the $NH_3$ desorption peaks arises at the same temperature. According to results shown in Fig. 2, the surface concentration of acid sites decreased, which might be due to the loading of nickel occupying the acidic sites on the zirconia surface.

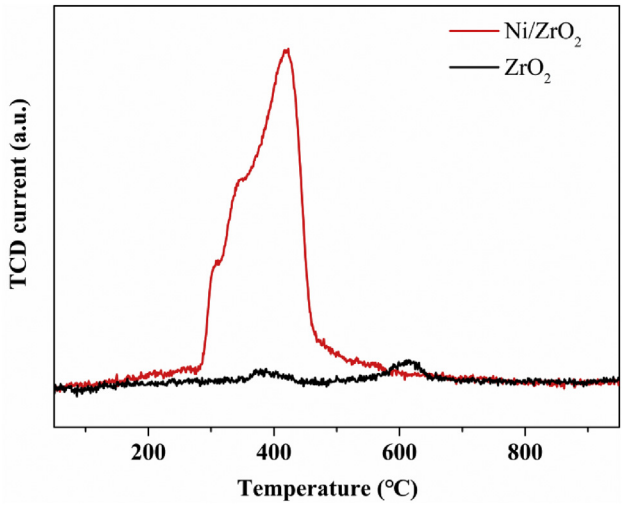


**Fig. 1 – $H_2$-TPR profile of $Ni/ZrO_2$ and $ZrO_2$.**

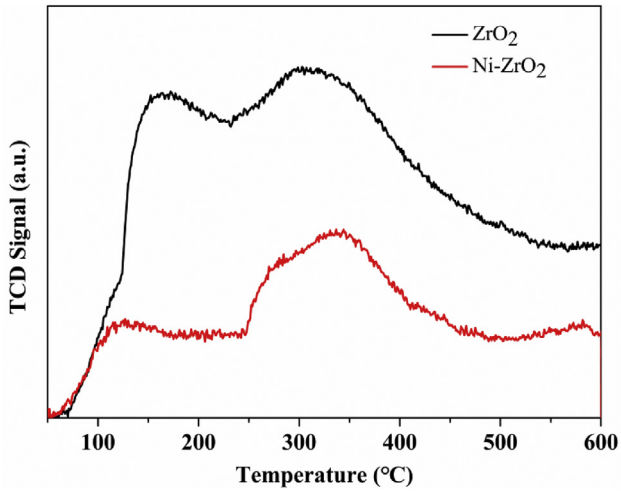


**Fig. 2 – $NH_3$-TPD profile of $Ni/ZrO_2$ and $ZrO_2$.**

### Catalytic activities

$X_{CH4}$, $C_{CO}$ and $C_{CO2}$ obtained at 550 °C were shown in Fig. 3. The initial $CH_4$ conversions (at 1 h) were 38.8%, 46.8%, 35.4%, 32.9% and 24.6%, and the yield of $H_2$ were 12.5%, 14.6%, 11.4%, 10.4% and 7.5% for the $H_2O$ to $CH_4$ ratio of 1, 2, 3, 5, 10, respectively. When the $H_2O/CH_4$ was 2, the highest conversion of methane was achieved. In terms of the content of CO and $CO_2$, when the $H_2O/CH_4$ was 1, $C_{co}$ (content of CO) was higher than $C_{co2}$ (content of $CO_2$). While the $H_2O/CH_4$ went above 1, $C_{co2}$ was higher than $C_{co}$. It was apparent that methane steam reforming reaction ($CH_4 + H_2O \rightarrow CO + 3H_2$) was carried out to a greater extent than the CO water vapor shift reaction ($CO + H_2O \rightarrow CO_2 + H_2$) [3,56–58] at lower $H_2O/CH_4$ ratio, and increasing the $H_2O/CH_4$ was more conducive to the following water gas shift reaction. In the 12-hour activity test, the catalysts with water-methane ratio of 1, 2 and 3 were gradually deactivated. When the $H_2O/CH_4$ was greater than 3, the catalyst deactivated more rapidly. Especially when the $H_2O/CH_4$ was 5 or 10, the catalyst was completely deactivated within 9 hours on steam. The stability of $Ni/TiO_2$ in SMR at $H_2O/CH_4$ ratios of 1–3 was studied and it was found that the catalyst would deactivate at the condition of $H_2O/CH_4 = 2$ [23]. As the steam feed was further increased ($H_2O/CH_4 = 3$), the greater presence of steam was capable of driving effective carbon gasification and re-stabilised SRM performance. And 45% methane conversion could be achieved at 500 °C. S. Gopalakrishnan et al. [59] found that when the reaction was carried out at $H_2O/CH_4 = 3$ on $Ni/CeZrO_2$, $H_2$ production was close to the thermodynamic upper limit in fact. In industrial applications, the ratio of water to methane was usually 2–5 [60,61]. In

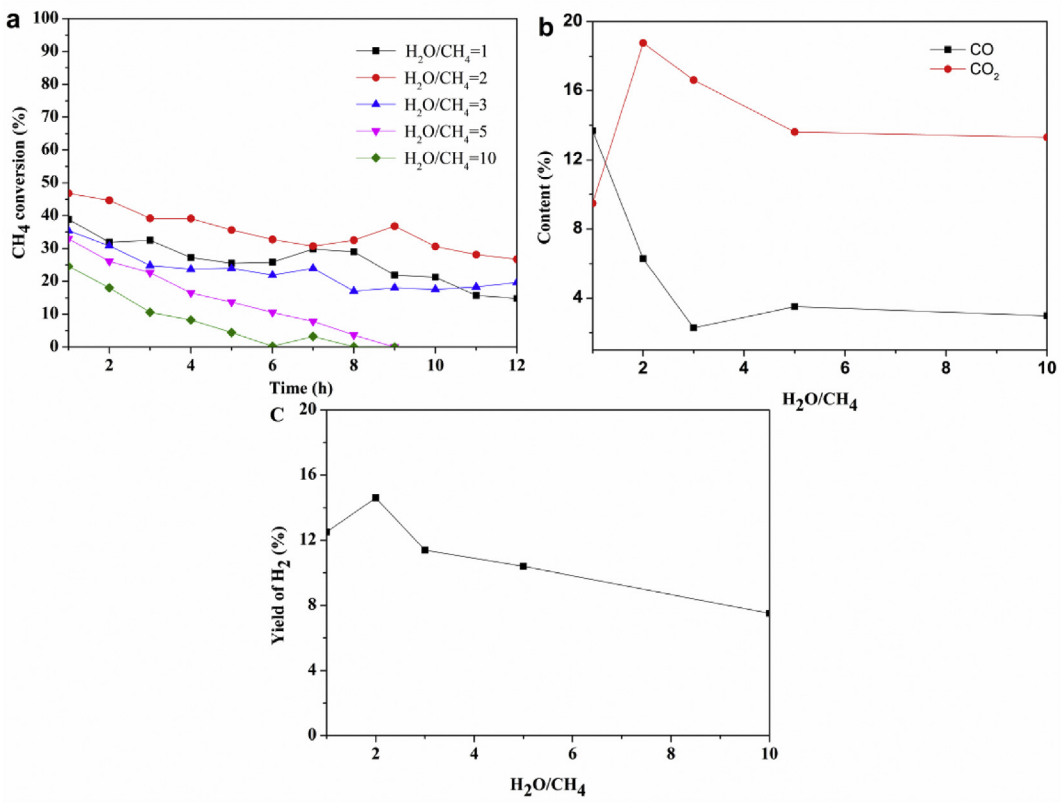


**Fig. 3 – Catalytic performance of Ni/$ZrO_2$ at 550 °C. (a) $CH_4$ conversion, (b) selectivity of CO and $CO_2$ and (c) yield of $H_2$ at 1st h.**

the literature, the optimal water-methane ratio was considered to be 3, while in this paper it was 2. The difference of the present work from literature might be caused by the different nature of the support used.

### *Characterization results*

Fig. 4 shows the XRD patterns after reduction and after reaction at different water to methane ratios. The diffraction peaks of nickel and zirconia both existed after reduction and after reaction. The crystallite size of nickel on Ni/$ZrO_2$ catalyst after reduction was 24 nm. Furthermore, the crystal size of metallic Ni after reaction at $H_2O/CH_4$ = 1, 2, 3, 5 or 10 were 23 nm, 28 nm, 22 nm, 22 nm, 22 nm respectively (Table 1), which showed no obvious variation of the size of Ni. When the $H_2O/CH_4$ was 2 or 3, the appearance of the diffraction peak of carbon indicated that a carbon species with better crystallinity was formed (38 nm and 28 nm). When the $H_2O/CH_4$ was 1, 5 or 10, there was no diffraction peak of carbon species on the XRD profiles. Ee Teng Kho et al. [23] investigated carbon deposition at different water to methane ratio and found the carbon peaks (2θ = 26.4°, 42.4°) from XRD results while $H_2O/CH_4$ = 2, and carbon whiskers appeared according to the TEM images on used catalysts which were not present in other ratios. It could be found that when the $H_2O/CH_4$ was 2 or 3, the same carbon species formed. Furthermore, it was not difficult to find that when the water-methane ratio was 2 and 3, the carbon peak appeared in the same position as the XRD results in the literature [23], and the presence of carbon whiskers were also found in the TEM image. This might mean that it was easy to form carbon whiskers at these water-methane ratios.

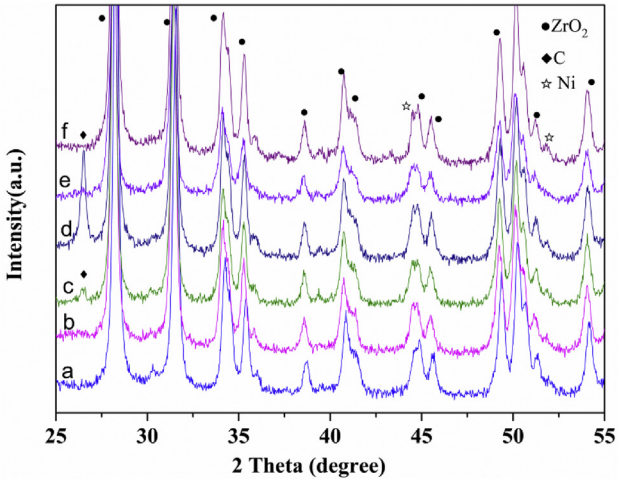


**Fig. 4 – XRD patterns of Ni/$ZrO_2$ (a) after reduction; after reaction, reaction condition: (b) $H_2O/CH_4$ = 1, (c) $H_2O/CH_4$ = 2, (d) $H_2O/CH_4$ = 3, (e) $H_2O/CH_4$ = 5, (f) $H_2O/CH_4$ = 10.**

TG-DSC-MS characterization was performed to study the deposited carbon on the used catalyst (Fig. 5). Carbon deposition could be divided into two types based on its different removal temperature, which included easy removal coke ($C_1$, Polymeric coke, removable at 400–500 °C) and difficult removal coke ($C_2$, Fiber carbon, removable at 500–600 °C) [48,62]. Obviously, when the $H_2O/CH_4$ was 1–3, there was $C_1$

**Table 1 – Amount of carbon deposition on used catalysts, characterized by TG-DSC-MS.**

| $H_2O/CH_4$ | Carbon deposition | | | | $W_{total}$ ($mg.g_{cat}^{-1}$) | Ni crystallite size(nm)[b] | conc. |
|---|---|---|---|---|---|---|---|
| | $C_1$ (peak 1) | | $C_2$ (peak 2) | | | | |
| | Position[a](°C) | $W_{C1}$ ($mg.g_{cat}^{-1}$)[c] | Position (°C) | $W_{C2}$ ($mg.g_{cat}^{-1}$) | | | $W_{C1}/W_{C2}$ |
| 1 | 471 | 73 | 564 | 78 | 151 | 23 | 0.93 |
| 2 | 436 | 26 | 564 | 21 | 47 | 28 | 1.24 |
| 3 | 434 | 17 | 556 | 11 | 28 | 22 | 1.54 |
| 5 | 471 | 13 | / | / | 13 | 22 | / |
| 10 | 436 | 11 | / | / | 11 | 22 | / |

$W_{C1}=W_{total}$*Weight Loss ratio(400–500 °C).
$W_{C2}=W_{total}$*Weight Loss ratio(500–600 °C).
[a] The center position of the peak on $CO_2$ MS single curve.
[b] Calculated from Ni [111] plane by the Scherrer equation.
[c] Calculated from the weight loss of TG (precision: 0.0001 mg).

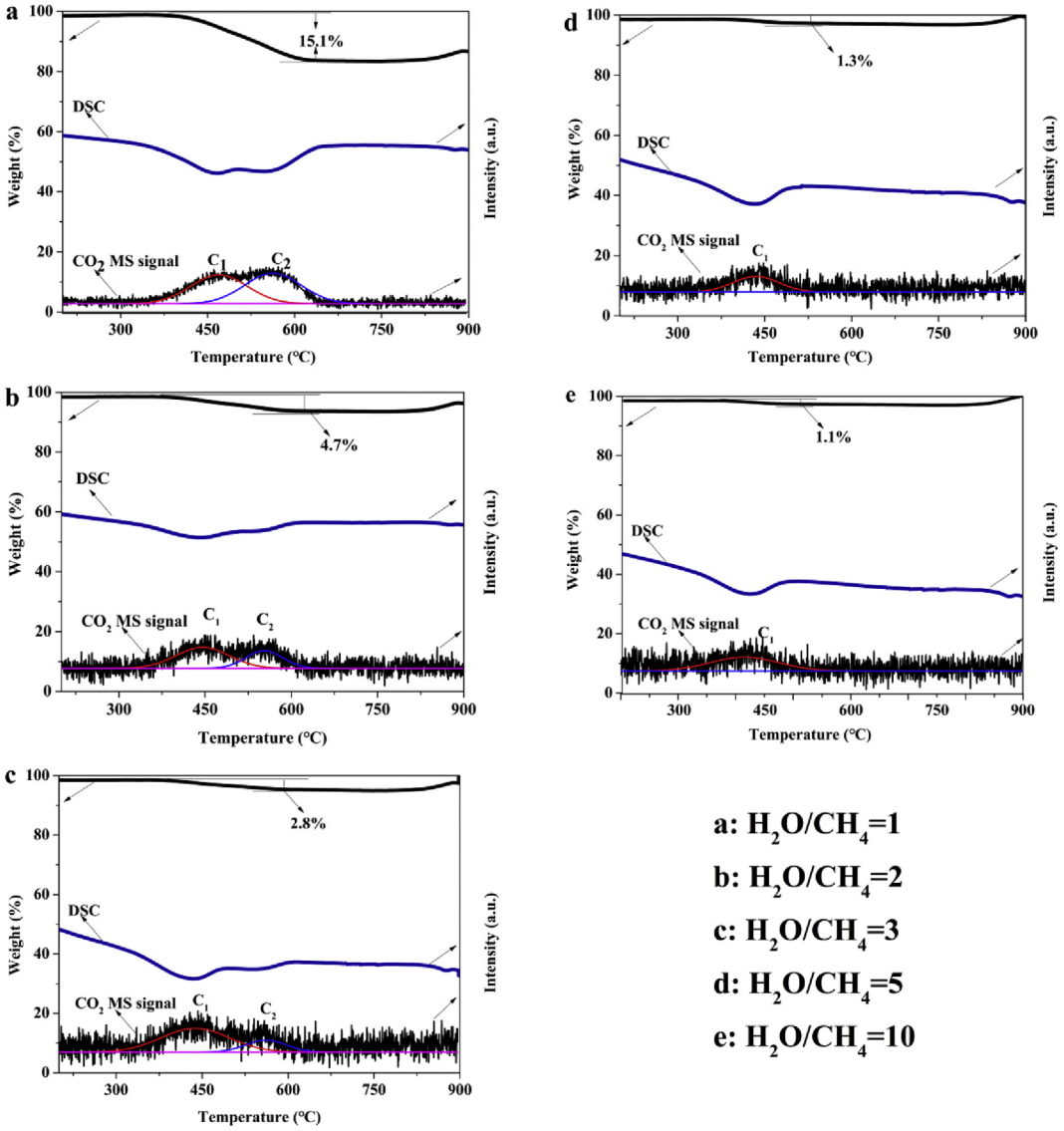


**Fig. 5 – TG-DSC-MS of $Ni/ZrO_2$ catalyst after reaction at different $H_2O/CH_4$.**

and $C_2$ carbon deposition, and when the $H_2O/CH_4$ was 5 or 10, there was only $C_1$ carbon deposition. The different amounts of carbon species were given in Table 1. When the ratio of water to methane increased, the amount of carbon accumulated decreased from 151 mg/g to 11 mg/g. This phenomenon indicated that a certain percentage of water in the feed had the ability to eliminate carbon [23,45]. Under the condition of $H_2O/CH_4$ of 1, the $C_2$ (78 mg.$g_{cat}^{-1}$) content was slightly higher than $C_1$ (73 mg.$g_{cat}^{-1}$). However, under the condition of $H_2O/CH_4$ of 2 and 3, the $C_2$ (21 mg.$g_{cat}^{-1}$and 11 mg.$g_{cat}^{-1}$) content was lower than $C_1$ (26 mg.$g_{cat}^{-1}$ and 17 mg.$g_{cat}^{-1}$). Under the condition of $H_2O/CH_4$ of 5 and 10, only small amount of $C_1$ coke (13 mg.$g_{cat}^{-1}$and 11 mg.$g_{cat}^{-1}$) was formed. $C_1/C_2$ increased with the increase of $H_2O/CH_4$, indicating that difficult removal coke ($C_2$) formed on used catalysts under lower $H_2O/CH_4$, expectantly, when $H_2O/CH_4 = 5$ or 10, only small easy removal coke ($C_1$) formed on the used catalysts. This suggested that large amounts of water can not only eliminate the $C_1$ species, but also inhibit the formation of $C_2$ species.

Furthermore, TG was used to characterize the generation of carbon deposit ($H_2O/CH_4 = 2$) at different reaction times (Fig. 6). In the first three hours of the reaction, weight loss was only found from 400 °C to 500 °C. From the fifth hour, the used catalyst exhibited weight loss over 500°C–600 °C range. Therefore, it could be concluded that when the ratio of water to methane was 2, $C_1$ carbon (removal temperature was 400–500 °C) was generated first, and then $C_2$ carbon (removal temperature was 500–600 °C) was generated as the reaction time increased. The weight loss rates of different temperature ranges were shown in Table 2.

It has been reported that polymer coke is thought to be derived from the thermal decomposition of hydrocarbons, while filamentous and graphite coke is formed over the catalyst [62]. When the ratio of water to methane was 2, the methane decomposition rate was expected to be high. As a consequence, the formation of amorphous coke was more likely very fast, since there was not sufficient water for carbon gasification. It have been reported that when the interaction of metal with the support was relatively weak, carbon deposition with higher graphitization degree could

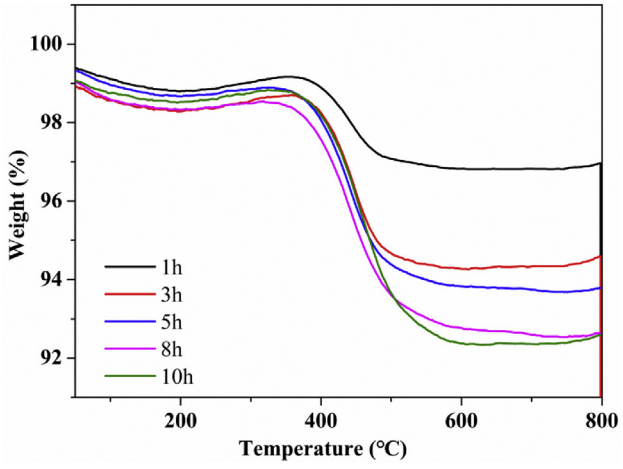


**Fig. 6 – The weight loss curve of the catalyst after the reaction at different reaction times($H_2O/CH_4 = 2$).**

**Table 2 – Amount of carbon deposition on used catalysts at different time ($H_2O/CH_4 = 2$), characterized by TG.**

| Time (h) | Carbon deposition | | |
|---|---|---|---|
| | 400–500 °C | 500–600 °C | Total weight loss (%) |
| | Weight loss (%)[a] | Weight loss (%) | |
| 1 | 1.82 | / | 1.82 |
| 3 | 3.58 | / | 3.58 |
| 5 | 3.68 | 0.55 | 4.23 |
| 8 | 3.95 | 0.84 | 4.79 |
| 10 | 4.53 | 1.27 | 5.80 |

[a] Calculated from the weight loss of TG (precision: 0.0001 mg).

be formed between Ni and the support [59,63–65]. With the increase of reaction time, the polymer carbon accumulated, and because Ni has weak interaction with the carrier, the carbon atoms will spread between the metal particles and the carrier to grow orderly carbon fibers [66]. The catalyst particles were lifted by the growing fiber carbon and their length was extended to promote the growth of fiber carbon at its tip [65].

TEM images of the $Ni/ZrO_2$ catalysts after reaction at 550 °C in different $CH_4/H_2O$ mixture were given in Fig. 7. It could be seen that when the $H_2O/CH_4$ were 1, 2 or 3, two kinds of carbon (polymer carbon and fiber carbon) were produced. When the $H_2O/CH_4$ was 5 and 10, only one kind of carbon ($C_1$) was produced. Especially, when the $H_2O/CH_4$ was 1, the flocculent carbon would cover the catalyst surface. This may lead to the blockage of catalytic and active sites, affecting catalytic activity [45,67].

XPS characterization was used to study the surface states of catalysts after reduction and reaction. The Ni $2p_{3/2}$ peak of $Ni/ZrO_2$ (seen in Fig. 8) after reduction was at 855.1 eV, which corresponded to the bulk of NiO species [19]. The results showed that the binding peaks of 855.8 eV and 852.3 eV both appeared on the $Ni/ZrO_2$ catalysts after reaction. It was reported that 852.3 eV was considered to be $Ni^0$ species and 855.8 eV was considered as $Ni(OH)_2$ species [19,32,68]. The results indicated that $Ni^0$ and $Ni(OH)_2$ co-existed on $Ni/ZrO_2$ catalysts after reaction. It was well-known that metallic Ni sites would activate C-H bonds [69,70]. This means that the higher content of $Ni^0$ species on the catalyst surface, the better the catalytic activity. Wang Y. et al. [48] found that when the $Ni^0$ on Ni-Zr/$SiO_2$ catalyst was oxidized to NiO for dry reforming of methane, it would result in its deactivation. NiO and Ni species might exist on the reduced catalyst. Then, it can be seen that Ni and $Ni(OH)_2$ existed on the catalyst after reaction from the XPS Ni 2p profile. The results of relative contents of different Ni species on the catalyst surface were shown in Table 3. When the $H_2O/CH_4$ was greater than 2, the $Ni^0$ content on the catalyst surface gradually decreased, and that of $Ni(OH)_2$ relatively increased, which indicated that a large amount of water would promote the conversion of $Ni^0$ to $Ni(OH)_2$. This may be due to the fact that the $Ni^0$ was oxidized into $Ni(OH)_2$ by water. In general, compared with $Ni/Ni(OH)_2$ on the surface of the catalyst under different $H_2O/CH_4$ after the reaction, it was not difficult to draw a conclusion that the surface reconstruction occurred on the catalyst.

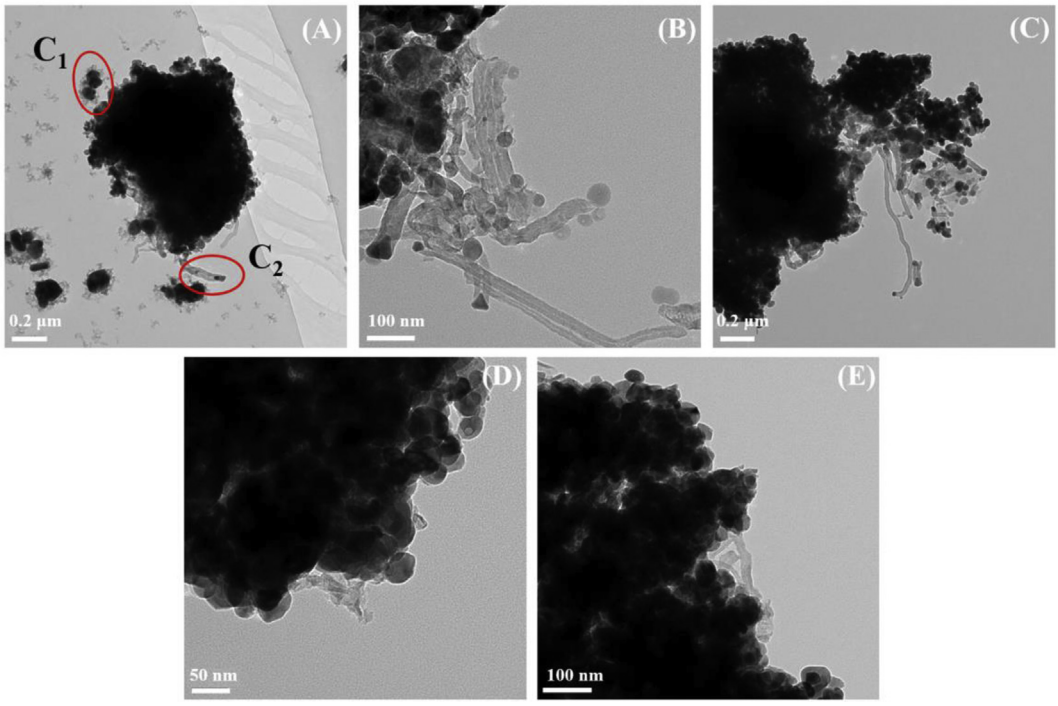


**Fig. 7 – TEM images of the Ni/$ZrO_2$ sample after testing in different $CH_4/H_2O$ mixture at 550 °C. $CH_4/H_2O$= (A) 1, (B) 2, (C) 3, (D) 5, (E) 10.**

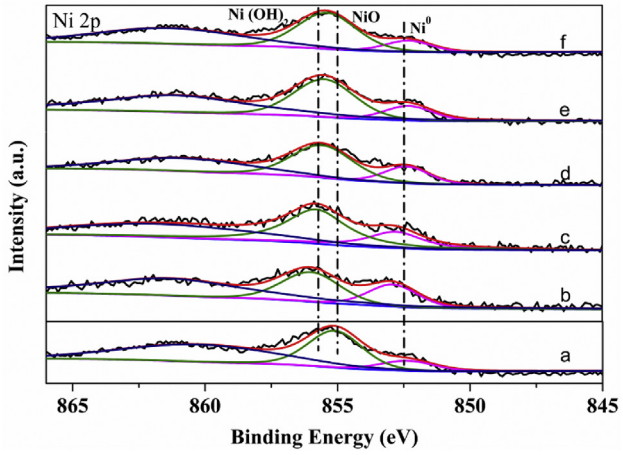


**Fig. 8 – Ni 2p binding energy of Ni/$ZrO_2$ (a) after reduction and after reaction at different $H_2O/CH_4$. (b) $H_2O/CH_4$ = 1; (c) $H_2O/CH_4$ = 2; (d) $H_2O/CH_4$ = 3; (e) $H_2O/CH_4$ = 5; (f) $H_2O/CH_4$ = 10.**

According to the data of C1s XPS (Fig. 9), when the ratio of water to methane was 1, 2 or 3, there are two different carbon peaks. Carbon at low binding energy was considered to be polymer carbon ($C_1$, BE = 284.6eV) overlapped with the contaminant carbon of the measurement system, while the carbon at high binding energy was considered to be fiber carbon ($C_2$, BE = 285.8eV). There were also two kinds of carbon deposition under the ratio of water to methane below 3 and there was only polymer carbon with $H_2O/CH_4$ = 5, 10 in XPS C 1s results, which was consistent with TG-MS results. In TG-MS results, the ratio of $C_1$ to $C_2$ increases with the $H_2O/CH_4$ ratio increasing. However, in the XPS results, the ratio of $C_1$ to $C_2$ (see in Table 3) decreased. It could be due to the fact that $C_1$ carbon deposition overlaps with the contaminant carbon (284.6eV) in XPS instrument, which would greatly affect the ratio of $C_1/C_2$. Thus, the XPS results just give one a qualitative tendency of carbon species deposited.

The O 1s peak of Ni/$ZrO_2$ (seen in Fig. 10) after reduction could be deconvoluted to 529.4 eV (lattice oxygen) and 530.8 eV (surface $OH^-$) [48]. Concerning the Ni/$ZrO_2$ after reaction under different condition, the peak of $Ni(OH)_2$ (531.2 eV)

**Table 3 – The XPS data analysis of different nickel and carbon species.**

| $H_2O/CH_4$ | $Ni^0$ | $Ni(OH)_2$ or NiO | Surface conc. $Ni^0/Ni(OH)_2$ or NiO | $C_2$ | $C_1$ | Surface conc. $C_1/C_2$ |
|---|---|---|---|---|---|---|
| | Area | Area | | Area | Area | |
| Reduction | 1026 | 3000 | 0.34 | / | / | / |
| 1 | 930 | 2570 | 0.36 | 2656 | 6686 | 2.51 |
| 2 | 1076 | 2843 | 0.38 | 3855 | 3129 | 0.82 |
| 3 | 843 | 2627 | 0.32 | 3654 | 2802 | 0.74 |
| 5 | 1023 | 3295 | 0.31 | 3755 | / | / |
| 10 | 870 | 3520 | 0.25 | 3643 | / | / |

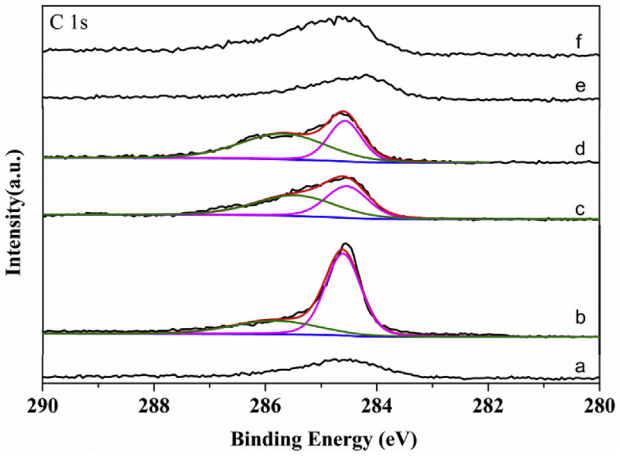


**Fig. 9 – C 1s binding energy of $Ni/ZrO_2$ (a) after reduction and after reaction at different $H_2O/CH_4$. (b) $H_2O/CH_4 = 1$; (c) $H_2O/CH_4 = 2$; (d) $H_2O/CH_4 = 3$; (e) $H_2O/CH_4 = 5$; (f) $H_2O/CH_4 = 10$.**

appeared [71]. Thus it confirmed that Ni combined with water to form $Ni(OH)_2$ on the surface. When the ratio of water to methane is less than 2, it is not difficult to find that the content of lattice oxygen decreases. This may contribute to the presence of oxygen defects on the surface of the catalyst to participate in the reaction, thereby facilitating the transfer of O from $ZrO_2$. When the water content increases, on the one hand, lattice oxygen is timely supplemented, on the other hand, excessive $H_2O$ will promote the transformation of $Ni^0$ to $Ni(OH)_2$.

Raman spectroscopy was used to study the graphitization degree of carbon deposition (Fig. 11). It had been reported that the four major bands (1348 $cm^{-1}$, 1578 $cm^{-1}$, 1604 $cm^{-1}$ and 2649 $cm^{-1}$) represented D band, G band, D'band and G'band respectively [72]. The D band was mainly regarded as the structural defects of defective carbon materials, whereas the G band was assigned to well-ordered graphitic carbon. The integrated intensities ratios of the G and D bands ($I_G/I_D$) of carbons

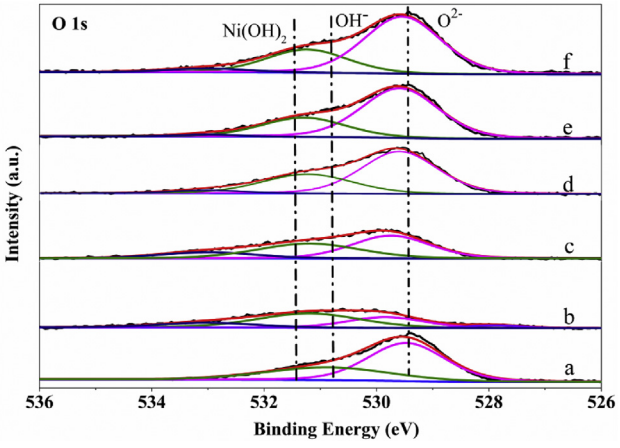


**Fig. 10 – O 1s binding energy of $Ni/ZrO_2$ (a) after reduction and after reaction at different $H_2O/CH_4$. (b) $H_2O/CH_4 = 1$; (c) $H_2O/CH_4 = 2$; (d) $H_2O/CH_4 = 3$; (e) $H_2O/CH_4 = 5$; (f) $H_2O/CH_4 = 10$.**

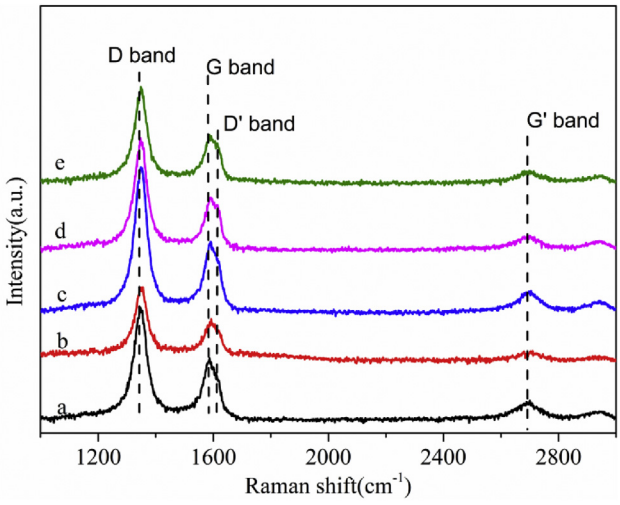


**Fig. 11 – Raman spectra of carbon deposition over the catalysts used with different $H_2O/CH_4$ ratio. (a) $H_2O/CH_4 = 1$, (b) $H_2O/CH_4 = 2$, (c) $H_2O/CH_4 = 3$, (d) $H_2O/CH_4 = 5$, (e) $H_2O/CH_4 = 10$.**

at different water to methane ratio ($H_2O$ = 1, 2, 3, 5, 10) were 0.59, 0.56, 0.53, 0.52 and 0.52, respectively. The carbon graphitization degree decreased gradually when the water to methane ratio increased. Carbon deposition with higher graphitization degree could be formed between Ni and the support [66]. When the amount of water was low, there were relatively more $Ni^0$ species on the surface which might result in a high methane decomposition rate. Since there was not sufficient water for carbon gasification, the rate of graphitization of carbon was greater than that of gasification. Thus the amount of graphitic carbon was relatively higher than that of polymer carbon. With high concentration of water, $Ni(OH)_2$ was formed, which lead to the diminution of the available surface metallic nickel. Therefore, the first step for coke formation, i.e., methane decomposition ($CH_4 \rightarrow C+2H_2$) would also diminish, which means that the total carbon deposition decreased. Furthermore, the high concentration of water also contributed to coke gasification. And the carbon atoms that spread through the metal particles to the other side of the fiber did not have time to grow to form ordered carbon fibers. So the amount of polymer carbon was greater than fiber carbon. This lead to a reduction in graphitization. Even at a water to methane ratio of 5, 10, only had little coke and it was mostly polymer carbon.

## Conclusion

The effect of $H_2O/CH_4$ on coke type over $Ni/ZrO_2$ for steam reforming of methane at low temperature was investigated. When $H_2O$ to $CH_4$ ratio was 2, the highest methane conversion could be achieved at 550 °C. In addition, the difference in $H_2O/CH_4$ produced different forms of deposited carbon on the catalyst with different removal capacities. When the $H_2O/CH_4$ was 1, 2 or 3, polymer carbon ($C_1$) and fiber carbon ($C_2$) were both formed on the catalyst. Especially, when the ratio was 1, too much easy to removal polymer carbon($C_1$) covered the active site which would reduce the catalytic activity. While

only polymer carbon ($C_1$) formed at high $H_2O/CH_4$ ratio(5, 10). That was due to the fact that the excess water would lead to the reconstruction of the catalyst surface and make the active $Ni^0$ species be transformed to $Ni(OH)_2$. This was also the reason why the catalyst gradually deactivated completely under the condition of water-methane ratio of 5, 10.

## Acknowledgements

This work financially support from the National Key R&D Program of China (2018YFB1501404) and the 111 Project (B17030)and the Fundamental Research Fund for Central Universities. The characterization of the products from Analytical and Testing Center of Sichuan University is greatly acknowledged.

## Appendix A. Supplementary data

Supplementary data to this article can be found online at https://doi.org/10.1016/j.ijhydene.2020.03.112.

## REFERENCES

[1] Kechagiopoulos PN, Angeli SD, Lemonidou AA. Low temperature steam reforming of methane: a combined isotopic and microkinetic study. Appl Catal B Environ 2017;205:238–53.
[2] Cheah SK, Massin L, Aouine M, Steil MC, Fouletier J, Gélin P. Methane steam reforming in water deficient conditions on Ir/$Ce_{0.9}Gd_{0.1}O_{2-x}$ catalyst: metal-support interactions and catalytic activity enhancement. Appl Catal B Environ 2018;234:279–89.
[3] Meshksar M, Rahimpour M, Daneshmand-Jahromi S, Hafizi A. Synthesis and application of cerium-incorporated SBA-16 supported Ni-based oxygen carrier in cyclic chemical looping steam methane reforming. Catalysts 2018;8:1–17.
[4] Xu J, Froment GF. Methane steam reforming, methanation and water-gas shift: 1. Intrinsic kinetics. AIChE J 1989;35:88–96.
[5] Settar A, Abboudi S, Lebaal N. Effect of inert metal foam matrices on hydrogen production intensification of methane steam reforming process in wall-coated reformer. Int J Hydrogen Energy 2018;43:12386–97.
[6] Chang X, Ma T, Wu R. Impact of urban development on residents' public transportation travel energy consumption in China: an analysis of hydrogen fuel cell vehicles alternatives. Int J Hydrogen Energy 2019;44:16015–27.
[7] Kaya Kemal, Hames Yakup. Two new control strategies: For hydrogen fuelsaving and extend the life cycle in the hydrogenfuel cell vehicles. Int J Hydrogen Energy 2019;44:18967–80. https://doi.org/10.1016/j.ijhydene.2018.12.111.
[8] Liu X, Reddi K, Elgowainy A, Lohse-Busch H, Wang M, Neha R. Comparison of well-to-wheels energy use and emissions of a hydrogen fuel cell electric vehicle relative to a conventional gasoline-powered internal combustion engine vehicle. Int J Hydrogen Energy 2020;45:972–83.
[9] El-Emam RS, Ozcan H. Comprehensive review on the techno-economics of sustainable large-scale clean hydrogen production. J Clean Prod 2019;220:593–609.
[10] dos Santos KG, Eckert CT, De Rossi E, Bariccatti RA, Frigo EP, Lindino CA, et al. Hydrogen production in the electrolysis of water in Brazil, a review. Renew Sustain Energy Rev 2017;68:563–71.
[11] Chen YT, Hsu CW. The key factors affecting the strategy planning of Taiwan's hydrogen economy. Int J Hydrogen Energy 2019;44:3290–305.
[12] Boudries R, Khellaf A, Aliane A, Ihaddaden L, Khida F. PV system design for powering an industrial unit for hydrogen production. Int J Hydrogen Energy 2014;39:15188–95.
[13] Dawood F, Anda M, Shafiullah GM. Hydrogen production for energy: an overview. Int J Hydrogen Energy 2020;45:3847–69.
[14] Zakaria K, Thimmappa R, Mamlouk M, Scott K. Hydrogen generation by alcohol reforming in a tandem cell consisting of a coupled fuel cell and electrolyser. Int J Hydrogen Energy 2020;45(15):8107–17. https://doi.org/10.1016/j.ijhydene.2020.01.123.
[15] Sasikumar G, Muthumeenal A, Pethaiah S, Nachiappan N, Balaji R. Aqueous methanol eletrolysis using proton conducting membrane for hydrogen production. Int J Hydrogen Energy 2008;33:5905–10.
[16] Barelli L, Bidini G, Gallorini F, Servili S. Hydrogen production through sorption-enhanced steam methane reforming and membrane technology: a review. Energy 2008;33:554–70.
[17] Abbas SZ, Dupont V, Mahmud T. Modelling of $H_2$ production in a packed bed reactor via sorption enhanced steam methane reforming process. Int J Hydrogen Energy 2017;42:18910–21.
[18] Ding H, Xu Y, Luo C, Wang Q, Shen C, Xu J, Zhang L. A novel composite perovskite-based material for chemical-looping steam methane reforming to hydrogen and syngas. Energy Convers Manag 2018;171:12–9.
[19] Wang S, Wang Y, Hu C. The effect of $NH_3 \cdot H_2O$ addition in Ni/SBA-15 catalyst preparation on its performance for carbon dioxide reforming of methane to produce $H_2$. Int J Hydrogen Energy 2018;43:13921–30.
[20] Littlewood P, Xie X, Bernicke M, Thomas A, Schomäcker R. $Ni_{0.05}Mn_{0.95}O$ catalysts for the dry reforming of methane. Catal Today 2015;242:111–8.
[21] Singha RK, Shukla A, Yadav A, Adak S, Iqbal Z, Siddiqui N, Bal R. Energy efficient methane tri-reforming for synthesis gas production over highly coke resistant nanocrystalline Ni–$ZrO_2$ catalyst. Appl Energy 2016;178:110–25.
[22] Moon DJ. Hydrogen production by catalytic reforming of gaseous hydrocarbons (methane & LPG). Energy Convers Manag 2019;193:39–51.
[23] Kho ET, Scott J, Amal R. Ni/$TiO_2$ for low temperature steam reforming of methane. Chem Eng Sci 2016;140:161–70.
[24] Hamid R, Radfarnia MCI. Development of Al-stabilized CaO–nickel hybrid sorbent–catalyst for sorption-enhanced steam methane reforming. Chem Eng Sci 2014;109:212–9.
[25] Agrafiotis CC, Pagkoura C, Lorentzou S, Kostoglou M, Konstandopoulos AG. Catal Today 2007;127:265–77.
[26] Halabi MH, de Croon MHJM, van der Schaaf J, Cobden PD, Schouten JC. Low temperature catalytic methane steam reforming over ceria–zirconia supported rhodium. Appl Catal A Gen 2010;389:68–79.
[27] Angeli SD, Pilitsis FG, Lemonidou AA. Methane steam reforming at low temperature: effect of light alkanes' presence on coke formation. Catal Today 2015;242:119–28.
[28] Kim HM, Jang WJ, Yoo SY, Shim JO, Jeon KW, Na HS, Lee YL, Jeon BH, Bae JW, Roh HS. Low temperature steam reforming of methane using metal oxide promoted Ni-$Ce_{0.8}Zr_{0.2}O_2$ catalysts in a compact reformer. Int J Hydrogen Energy 2018;43:262–70.
[29] Tsang SC, Claridge JB, Green MLH. Recent advances in the conversion of methane to synthesis gas. Catal Today 1995;23:3–15.

[30] Yu X, Zhang F, Wang N, Hao S, Chu W. Plasma-treated bimetallic Ni-Pt catalysts derived from hydrotalcites for the carbon dioxide reforming of methane. Catal Lett 2014;144:293–300.
[31] Angeli SD, Pilitsis FG, Lemonidou AA. Methane steam reforming at low temperature: effect of light alkanes' presence on coke formation. Catal Today 2015;242:119–28.
[32] Fang X, Zhang X, Guo Y, Chen M, Liu W, Xu X, Peng H, Gao Z, Wang X, Li C. Highly active and stable Ni/$Y_2Zr_2O_7$ catalysts for methane steam reforming: on the nature and effective preparation method of the pyrochlore support. Int J Hydrogen Energy 2016;41:11141–53.
[33] Rajib KS, Astha S, Aditya Y, Shubhadeep A, Zafar I, Nazia S, Rajaram B. Energy effificient methane tri-reforming for synthesis gas production over highly coke resistant nanocrystalline Ni–$ZrO_2$ catalyst. Appl Energy 2016;78:110–25.
[34] Wei J, Iglesia E. Isotopic and kinetic assessment of the mechanism of reactions of $CH_4$ with $CO_2$ or $H_2O$ to form synthesis gas and carbon on nickel catalysts. J Catal 2004;224:370–83.
[35] Jarrah NA, van Ommen JG, Lefferts L. Mechanistic aspects of the formation of carbon-nanofibers on the surface of Ni foam: a new microstructured catalyst support. J Catal 2006;239:460–9.
[36] Vang RT, Honkala K, Dahal S, Vestergaard EK, Schnadt J, Lægsgaard E, Clausen BS, Nørskov JK, Besenbacher F. Controlling the catalytic bond-breaking selectivity of Ni surfaces by step blocking. Nat Mater 2005;4:160–2.
[37] Dong WS, Roh HS, Jun KW, Park SE, Oh YS. Methane reforming over Ni/Ce-$ZrO_2$ catalysts: effect of nickel content. Appl Catal A 2002;226:63–72.
[38] Roh HS, Eum IH, Jeong DW. Low temperature steam reforming of methane over Ni–$Ce_{(1-x)}Zr_{(x)}O_2$ catalysts under severe conditions. Renew Energy 2012;42:212–6.
[39] Carvalho LS, Martins AR, Reyes P, Oportus M, Albonoz A, Vicentini V, do Rangel MC. Preparation and characterization of Ru/MgO-$Al_2O_3$ catalysts for methane steam reforming. Catal Today 2009;142:52–60.
[40] Sehested J. Four challenges for nickel steam-reforming catalysts. Catal Today 2006;111:103–10.
[41] Roy PS, Raju ASK, Kim K. Influence of S/C ratio and temperature on steam reforming of model biogas over a metal-foam-coated Pd–Rh/($CeZrO_2$–$Al_2O_3$) catalyst. Fuel 2015;139:314–20.
[42] Großmann K, Treiber P, Karl J. Steam methane reforming at low S/C ratios for power-to-gas applications. Int J Hydrogen Energy 2016;41:17784–92.
[43] Iglesias I, Forti M, Baronetti G, Mariño F. Zr-enhanced stability of ceria based supports for methane steam reforming at severe reaction conditions. Int J Hydrogen Energy 2019;44:8121–32.
[44] Nieva MA, Villaverde MM, Monzón A, Garetto TF, Marchi AJ. Steam-methane reforming at low temperature on nickel-based catalysts. Chem Eng J 2014;235:158–66.
[45] Kowit Lertwittayanon WY, Woei JL. Enhanced catalytic performance of Ni/α-$Al_2O_3$ catalyst modified with CaZrO3 nanoparticles in steam-methane reforming. Int J Hydrogen Energy 2017;42:28254–65.
[46] Gonzalez-Delacruz VM, Perenïguez R, Ternero F, Holgado JP, Caballero A. Modifying the size of nickel metallic particles by $H_2$/CO treatment in Ni/$ZrO_2$ methane dry reforming catalysts. ACS Catal 2011;1:82–8.
[47] Eder D, Kramer R. The stoichiometry of hydrogen reduced zirconia and its influence on catalytic activity. Phys Chem Chem Phys 2002;4:795–801.
[48] Wang Y, Yao L, Wang Y, Wang S, Zhao Q, Mao D, Hu C. Low-temperature catalytic $CO_2$ dry reforming of methane on Ni-Si/$ZrO_2$ catalyst. ACS Catal 2018;8:6495–506.
[49] Yao L, Shi J, Xu H, Shen W, Hu C. Low-temperature $CO_2$ reforming of methane on Zr-promoted Ni/$SiO_2$ catalyst. Fuel Process Technol 2016;144:1–7.
[50] Sutthiumporn K, Maneerung T, Kathiraser Y, Kaw S. CO2 dry-reforming of methane over $La_{0.8}Sr_{0.2}Ni_{0.8}M_{0.2}O_3$ perovskite (M = Bi, Co, Cr, Cu, Fe): roles of lattice oxygen on C-H activation and carbon suppression. Int J Hydrogen Energy 2012;37:11195–207.
[51] Jia X, Zhang X, Rui N, Hu X, Liu CJ. Structural effect of Ni/$ZrO_2$ catalyst on $CO_2$ methanation with enhanced activity. Appl Catal B Environ 2019;244:159–69.
[52] Pérez-Hernández R, Mondragón Galicia G, Anaya DM, Palacios J, Angeles-Chavez C, Arenas-Alatorre J. Synthesis and characterization of bimetallic Cu–Ni/$ZrO_2$ nanocatalysts: H2 production by oxidative steam reforming of methanol. Int J Hydrogen Energy 2008;33:4569–76.
[53] Roh HS, Jun KW, Dong WS, Chang JS, Park SE, Joe YI. Highly active and stable Ni/Ce–$ZrO_2$ catalyst for $H_2$ production from methane. J Mol Catal Chem 2002;81:137–42.
[54] Hu Y, Jin S, Zhang Z, Zhang L, Deng J, Zhang H. One-step synthesis of nitriles by the dehydrogenation–amination of fatty primary alcohols over Cu/m-$ZrO_2$. Catal Commun 2014;54:45–9.
[55] Ainul HK, Sugeng T, Aishah AJ, Hideshi H. $WO_3$ monolayer loaded on $ZrO_2$: property–activity relationship in n-butane isomerization evidenced by hydrogen adsorption and IR studies. Appl Catal A Gen 2012;433:49–57.
[56] Ochoa-Fernández E, Haugen G, Zhao T, Rønning M, Aartun I, Børresen B, Rytter E, Rønnekleiv M, Chen D. Process design simulation of $H_2$ production by sorption enhanced steam methane reforming: evaluation of potential $CO_2$ acceptors. Green Chem 2007;9:654–62.
[57] Gonçalves JF, Souza MMVM. Effect of doping niobia over Ni/$Al_2O_3$ catalysts for methane steam reforming. Catal Lett 2018;148:1478–89.
[58] Antonio Ricca VP, Marco M, Eugenio M. Innovative catalyst design for methane steam reforming intensification. Fuel 2017;198:175–82.
[59] Gopalakrishnan S, Faga MG, Miletto, Coluccia S, Caputo, Sau GS, Giaconia A, Berlier G. Unravelling the structure and reactivity of supported Ni particles in Ni-$CeZrO_2$ catalysts. Appl Catal B Environ 2013;138:353–61.
[60] Berman A, Karn RK, Epstein M. Kinetics of steam reforming of methane on Ru/$Al_2O_3$ catalyst promoted with Mn oxides. Appl Catal 2005;282:73–83.
[61] Pistonesi C, Juan A, Irigoyen B, Amadeo N. Theoretical and experimental study of methane steam reforming reactions over nickel catalyst. Appl Surf Sci 2007;253:4427–37.
[62] Guo J, Lou H, Zheng X. The deposition of coke from methane on a Ni/$MgAl_2O_4$ catalyst. Carbon 2007;45:1314–21.
[63] Jehng JM, Tung WC, Kuo CH. The formation mechanisms of multi-wall carbon nanotubes over the Ni modified MCM-41 catalysts. J Porous Mater 2008;15(1):43–51.
[64] Lee CJ, Park J. Growth model of bamboo-shaped carbon nanotubes by thermal chemical vapor deposition. Appl Phys Lett 2000;77:3397–9.
[65] Saraswat SK, Pant KK. Ni-Cu-Zn/MCM-22 catalysts for simultaneous production of hydrogen and multiwall carbon nanotubes via thermo-catalytic decomposition of methane. Int J Hydrogen Energy 2011;13:13352–61.
[66] Endo M, Kroto HW. Formation of carbon nanofibers. J Phys Chem 1992;96:6941–4.
[67] Aparicio LM. Transient isotopic studies and microkinetic modeling of methane reforming over nickel catalysts. J Catal 1997;165:262–74.
[68] Németh M, Schay Z, Srankó D, Károlyi J, Sáfrán G, Sajó I, Horváth A. Impregnated Ni/$ZrO_2$ and Pt/$ZrO_2$ catalysts in dry reforming of methane: activity tests in excess methane and

mechanistic studies with labeled $^{13}CO_2$. Appl Catal A Gen 2015;504:608–20.

[69] Liu H, Wierzbicki D, Debek R, Motak M, Grzybek T, Costa PD, Galvez ME. La-promoted Ni-hydrotalcite-derived catalysts for dry reforming of methane at low temperatures. Fuel 2016;182:8–16.

[70] Wei J, Iglesia E. Isotopic and kinetic assessment of the mechanism of reactions of $CH_4$ with $CO_2$ or $H_2O$ to form synthesis gas and carbon on nickel catalysts. J Catal 2004;224:370–83.

[71] Thawatchai M, Kus H, Sibudjing K. Co-production of hydrogen and carbon nanofibersfrom catalytic decomposition of methane over $LaNi_{(1-x)}MxO_{3-\alpha}$ perovskite (where M= Co, Fe and X= 0, 0.2, 0.5, 0.8, 1). Int J Hydrogen Energy 2015;40:13399–411.

[72] Yao L, Shi J, Hu C. The structure, carbon deposition and stability of a ZrOx/Ni–MnOx/$SiO_2$ catalyst for the $CO_2$ reforming of methane. RSC Adv 2015;5:90168–77.